Performance Improvement in High-Performance Brushless Rare-Earth Magnet Motors for Hybrid Vehicles by Use of High Flux-Density Steel

David G. Dorrell[1], Andrew M. Knight[2], and Mircea Popescu[3]

[1]School of Electrical, Mechanical and Mechatronic Systems, University of Technology Sydney, Sydney, N.S.W. 2007, Australia
[2]Department of Electrical and Computer Engineering, University of Alberta, Edmonton, AB T6G 2V4 Canada
[3]Motor Design, Ltd., Ellesmere, Shropshire SY12 0EG, U.K.

Hybrid and electrical vehicles use mostly high-efficiency brushless permanent-magnet AC motors and sinewave drives. The motors utilize rare-earth magnet material and also are required to have a very high torque-per-rotor volume. The designs are now very well refined and often use interior permanent-magnet (IPM) rotors for a better field weakening control. This configuration has been shown to increase the efficiency. In this paper, the Toyota Prius 2004 motor is modeled using finite element analysis with different laminated steel materials in order to assess the effectiveness of using high flux-density steel versus the material volume. Additionally to the IPM rotor in the manufactured design, a spoke magnet rotor is also investigated. It is found that using high flux-density laminated steel will either increase the performance of the motor or allow the motor to be reduced in size (in this case, reduction in axial length).

***Index Terms*—Hybrid electric vehicle, brushless AC motor, interior permanent-magnet (IPM) rotor, high flux steel, efficiency.**

I. Introduction

MODERN hybrid-electric and electric vehicles (HEVs and EVs) use high-performance motor drives. The Toyota Prius is the most popular hybrid car and has been through several variants and upgrades over several years. The brushless permanent magnet motor for the 2004 model version was detailed by Oak Ridge Labs [1] (a cross section from the *SPEED* model of the machine is shown in Fig. 1). This is an eight-pole motor that operates up to about 6000 r/min. In [1], the design and performance investigation was compared to the Toyota Camry hybrid vehicle drive motor. This vehicle is a later development and a larger vehicle; it is interesting to note that the Camry machine is a similar size and design, but extra power is obtained by increasing the speed to 12 000 r/min. However, in this paper, the Prius 2004 motor is investigated since it is a more commonly known hybrid vehicle example. Analyses of this machine have been published elsewhere [2]–[5] with respect to analysis techniques and alternative designs (both IPM and non-IPM motor types). This paper builds on this literature and assesses the motor performance in terms of materials used and also addresses an alternative spoke design. This type of machine was investigated in [6].

While novel permanent-magnet machines such as that in [7] are being investigated, the standard radial-flux slotted-stator machine, with some variant on the IPM rotor, is still the preferred production machine. Replacements for this machine are likely to be induction (which have been used in EVs [8]) or reluctance machines [9], [10] due to concerns over rare-earth magnet material supply [11]. However, if supply-chain issues are resolved then high-performance drives in HEVs and EVs may well continue to be of an IPM motor arrangement in the majority of cases due to their high efficiency and torque density.

Manuscript received February 21, 2011; accepted May 03, 2011. Date of current version September 23, 2011. Corresponding author: D. G. Dorrell (e-mail: david.dorrell@uts.edu.au).

Color versions of one or more of the figures in this paper are available online at http://ieeexplore.ieee.org.

Digital Object Identifier 10.1109/TMAG.2011.2157103

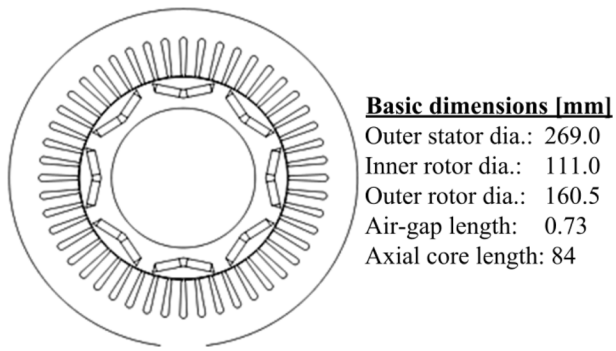

Fig. 1. *SPEED* PC-BDC representation of Prius 2004 drive motor.

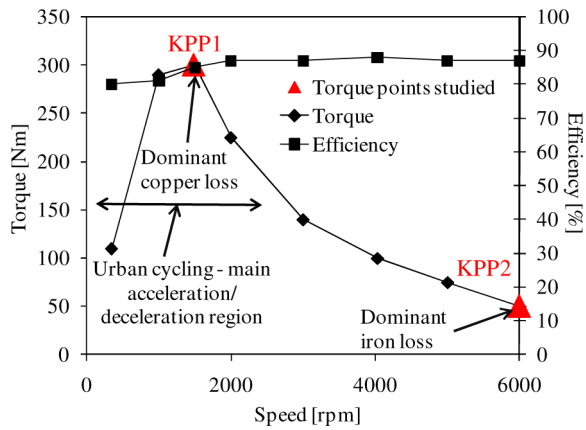

Fig. 2. Measured torque and efficiency envelopes for 2004 Prius PM drive motor [1]. The key performance points (KPPs) are shown.

II. Simulations

A. Prius Performance Envelope

The performance envelope of the Prius 2004 motor is shown in Fig. 2. These are for the motor torque measured in the Oak Ridge report [1]. This motor operates with a very wide field weakening range, with the main operation likely to be from 0 to 2000 r/min, which is the acceleration/deceleration urban cycle. Over this speed range, efficiency is very important. The machine

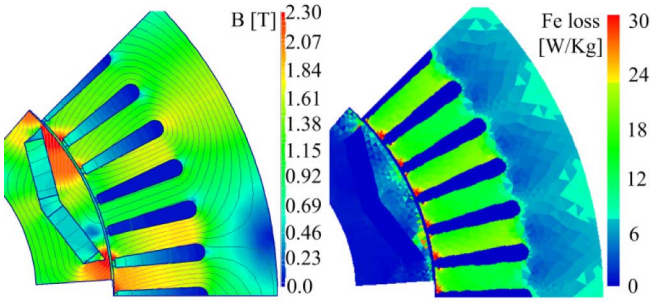

Fig. 3. Flux-density (left) and iron loss (right) distributions at 1500 r/min with 145-A root mean square (rms) and 60° phase advance.

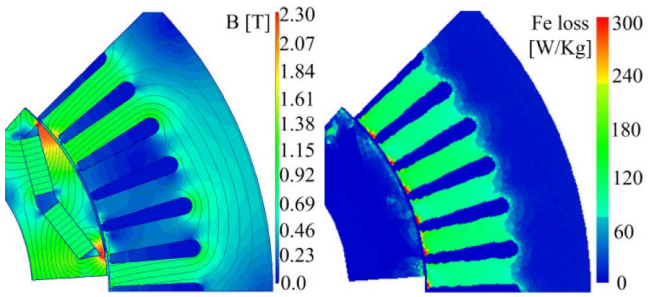

Fig. 4. Flux-density (left) and iron loss (right) distributions at 6000 r/min with 34.5-A rms and 60° phase advance.

is operating at high torque but low frequency so that copper loss is the dominant loss. At high speed, iron loss is dominant since the torque (and current) demand is lower.

This machine operates permanently at about 60° phase advance. Figs. 3 and 4 show instantaneous flux plots and the iron loss distribution calculated at key performance points KPP1 and KPP2. The most important point is KPP1. This will have a major effect on the drive performance; it has to be emphasized that KPP2 will only affect high end performance and probably only reduce the vehicle top speed slightly, which is rarely used, whereas the urban cycle is vitally important to performance assessment for most vehicles.

Fig. 1 illustrates that there is high q-axis saliency. The machine was studied in [2] and [3] and this showed that the phase advance considerably enhances the performance. Fig. 5 shows the breakdown of the excitation and reluctance torques at the two key operating points in Fig. 2 with a variation of phase advance angle of the current phasor. It illustrates that the peak torque is not at the same position due to saturation effects however 60° phase advance represents a good phase advance at KPP1 and KPP2. It is also possible to start the machine even with this phase advance as illustrated in [1].

Fig. 5 illustrates that the performance prediction can be difficult in these high-performance machines and different torque calculations can give very different results. In Fig. 5, finite element solutions are used to calculate the torque, but for the excitation, reluctance and total torques, dq-axis theory is used where the "frozen permeability" [12] method was applied to separate the excitation and reluctance torque. The dq equation [13] is

$$T = 3p(\Psi_d I_q - \Psi_q I_d) \tag{1}$$

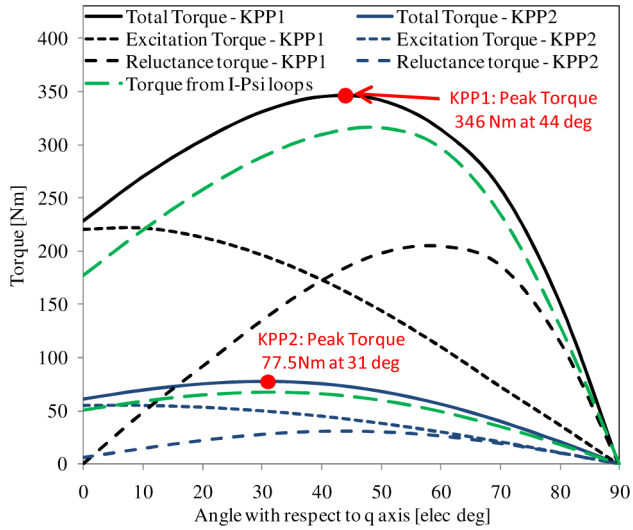

Fig. 5. Separation of torque at KPP1 (1500 r/min, 145 A) and KPP2 (6000 r/min, 35.4 A) loading using dq torque calculation method—variation of current phase with respect to q-axis. I-Psi calculation included for comparison.

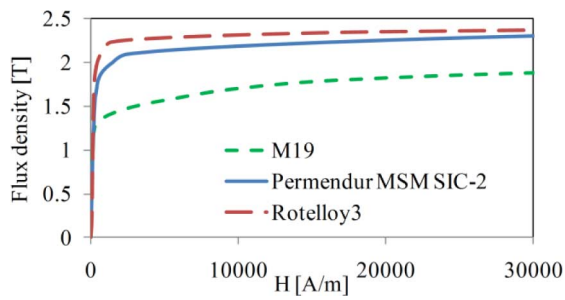

Fig. 6. Comparison of high flux-density steel with standard M19.

where p is the pole-pair number and Ψ is the d- and q-axis flux linkage phasors. For more accurate results the current and rotor should be stepped round together and the flux linkage obtained to form a current–flux-linkage (I-Psi) loop. The area enclosed is the energy conversion for one electrical cycle and this can be used to obtain the torque. Under saturated conditions (particularly KPP1) there is quite a divergence in calculations. The results in the following sections use I-Psi loops for a greater accuracy.

B. High Flux Steel Operation

It was found that the most demanding point occurs at the KPP1 as discussed in the previous section. Even though this is a high-efficiency point there is still considerable copper loss. The machine operates with 60° phase advance and there is high reluctance torque (Fig. 5). The effect of using high flux-density steel is studied here as a way of improving machine operation and reducing the copper loss. In [2]–[5], M19 24 gage steel was used; in this paper, Rotelloy 3 is introduced as an option; this will allow either increased torque or reduction in size.

Different steel B/H curves are shown in Fig. 6. It is necessary to use the correct steel B/H curve for a machine of this ilk because it is driven well into saturation. The curve should extend well above the knee point as shown. The two high flux-density steels are Permendur SIC-2 from MSM, and Rotelloy 3,

TABLE I
OPERATION AT 1500 r/min (KPP1) WITH 60° ELEC. PHASE ADVANCE AT HIGH LOAD (REDUCED AXIAL LENGTH FROM 84 TO 68 mm)

Steel Type	M19	Rotelloy 3	Rotelloy 3 (reduced axial length)
V_{ph}(rms) [V]	182	196.7	175.9
I_{ph}(rms) [I]	190.9	157.7	190.9
P_{in} [kW]	67.6	65.8	66.1
Copper Loss [kW]	7.9	5.4	7.2
Iron Loss [kW]	0.2	0.19	0.16
Torque [Nm]	379	383	374
Efficiency [%]	88.0	91.4	88.8

TABLE II
OPERATION AT 6000 r/min (KPP2) WITH 60° ELEC. PHASE ADVANCE AT 60-Nm LOAD

Steel Type	M19	Rotelloy 3
V_{ph}(rms) [V]	302	303
I_{ph}(rms) [I]	35.4	35.4
P_{in} [kW]	32.9	32.4
Copper Loss [kW]	0.27	0.27
Iron Loss [kW]	0.95	0.39
Torque [Nm]	50.4	50.9
Efficiency [%]	96.4	97.9

which is similar to Vanadium Permendur 49Co/49Fe/2V. In the simulations below, Rotelloy 3 is used and I-Psi loops obtained from finite element analysis to calculate the torque. The machine windings and magnets were set to 100 °C while the air-gap was set to 80 °C in *SPEED* PC-BDC (brushless PM machine simulation package from the University of Glasgow, U.K. [14]) and PC-FEA (the finite element analysis bolt-on package). The cooling system is important in this type of machine but this paper is concerned with the electromagnetic performance.

The following sections analyze the IPM motor using M19 24 Gage and Rotelloy 3 at KPP1 and KPP2.

1) Low-Speed Operation—KPP1: The machine was simulated in *SPEED* PC-BDC. The torque was set to a nominal 400 Nm from PC-BDC (higher that the designated point in Fig. 1 to allow for overload) to obtain comparative results between M19 24 Gage and Rotelloy3. The torques obtained from the I-Psi loops were below the nominal due to the use of more accurate finite element analysis calculations. Table I puts forward the performance improvements with high flux-density steel. Rotelley3 will have lower loss density characteristics; however, at 1500 r/min, these losses are negligible. While there is only 3.4% improvement in efficiency this is an absolute reduction of 2.5 kW in loss which is concentrated in the motor coils. This will have a significant effect on the heating of the machine during the urban cycle.

An alternative is to maintain the current and torque and reduce the axial length. This will reduce the loss but also reduce the material. Both the steel and magnet are expensive. The axial length was reduced from 84 to 68 mm and the results are shown in Table I. It can be seen that there is a reduction in copper loss but not sufficient to change the efficiency to any great extent (<1%). This is obviously more of an exercise in material and size reduction rather than efficiency improvement. The material, both in terms of magnet material and expensive high flux steel, is reduced by 19%. This is a reasonably large change in the required material. Therefore, the increase in steel cost can be offset by reduction in magnet material and actual amount of steel used. There will also be some reduction in copper.

2) High-Speed Operation—KPP2: To address higher speed operation the simulation was run at 6000 r/min where the maximum required torque is about 50 Nm. The results are shown in Table II and these show little difference. This is because the electric loading is not high and the laminated steel in machine is not highly saturated. Therefore, it can be seen that the use of high flux-density steel is most relevant to KPP1. However, as already stated, KPP1 is the most important operation point. If the axial length is reduced then it is straightforward to increase the current to produce the required torque.

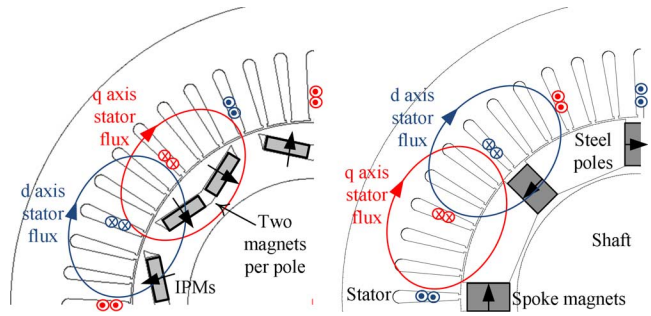

Fig. 7. 2004 Prius IPM motor cross section (left) and alternative spoke IPM (right) in *SPEED* PC-BDC—this shows two magnets per pole for the Prius motor, one magnet per pole for the spoke IPM, and high saliency in both cases.

III. SPOKE MAGNET ALTERNATIVE DESIGN

A. Comparison With IPM Machine

In this section, comparison is made with the spoke IPM machine shown in Fig. 7. The figure illustrates the saliency for both machines. The torque is compared directly (using I-Psi loops for accuracy) at KPP1 and KPP2. At KPP1 the current is kept constant at 145 A, while it is kept constant at 35.4 A at KPP2. The results with variation of current phasor with respect to the advance angle from q-axis are shown in Fig. 8. It can be seen that the spoke motor has a slightly different profile but offers a similar performance. The copper loss is constant and the iron losses are similar. This is a first pass arrangement and the magnet weight is kept constant. Flux plots for KPP1 and KPP2 are shown in Fig. 9. The phase advance is 60° in both instances. This arrangement represents an alternative to design to the IPM machine.

B. Use of High Flux-Density Steel

Table III gives a similar set of simulations for the spoke magnet arrangement to Table I for the IPM motor at KPP1. Again, the simulation is carried out at a higher current level to

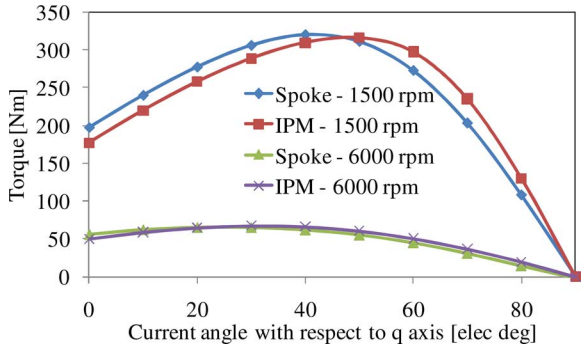

Fig. 8. Comparison for IPM and Spoke motor torques in Fig. 7 at KPP1 and KPP2 with the same currents.

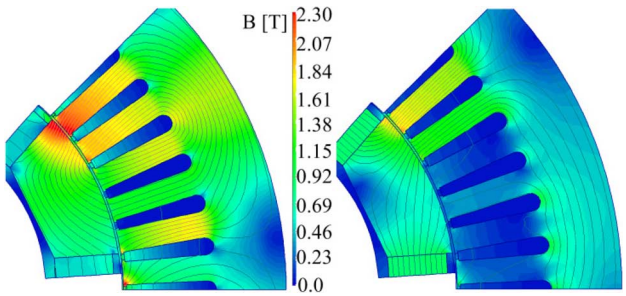

Fig. 9. Flux plots for Spoke machine at KPP1(left) and KPP2 (right); same flux-density scale is used for both configurations.

TABLE III
OPERATION AT 1500 r/min (KPP1) WITH 60° ELEC. PHASE ADVANCE AT HIGH LOAD (REDUCED AXIAL LENGTH FROM 84 TO 68 mm)

Steel/Motor Type	M19/ IPM motor	M19/ Spoke motor	Rotelloy 3/ Spoke motor	Rotelloy 3/ Spoke motor (reduced axial length)
V_{ph}(rms) [V]	182	172	179	159
I_{ph}(rms) [I]	190.9	190.9	170	190.9
P_{in} [kW]	67.6	67.5	66.9	63.5
Copper Loss [kW]	7.9	7.9	6.2	7.2
Iron Loss [kW]	0.2	0.1	0.07	0.06
Torque [Nm]	379	379	386	358
Efficiency [%]	88.0	88.1	90.5	88.6

allow for overload conditions. At 190.9 A, it can be seen that the IPM and spoke motors give almost identical simulation results. The improvement in performance with the high flux-density steel is not too significant. The machine requires higher current (170 A compared to 157.7 A) when the geometry is unchanged. This leads to minor efficiency increase. For the reduced axial length simulation, the current was kept constant with the same axial length reduction compared to the IPM motor. The torque is lower (358 Nm compared to 374 Nm for the IPM motor). Therefore, high flux-density steel is less effective for this arrangement. KPP2 simulations are not presented here as this point is not affected.

IV. CONCLUSION

This paper demonstrates that the use of high flux-density laminated steels can increase the performance of an IPM motor that is used in an HEV. For the IPM motor, it would lead to an important (19% for analyzed motor) reduction in magnet and steel material. This is a considerable material and mass saving and a compact power unit. While high flux-density steel may be too expensive for such an application, future material costs may reduce and also it may be possible the use of expensive materials in high-end sport or luxury vehicles. Currently its cost and scarcity means it is limited to aeronautical applications. The reduced mass may lead to further total vehicle drive cycle efficiency improvements. An alternative spoke rotor arrangement is investigated. This arrangement uses a similar volume of magnet material to the IPM configuration but may represent a more straightforward assembly since there is half the number of magnet blocks. The use of high flux-density steel is not quite as effective as may be assumed, but there is still an improvement in performance.

REFERENCES

[1] M. Olszewski, "Evaluation of the 2007 Toyota Camry hybrid synergy drive system," Oak Ridge Nat. Lab., U.S. Dept. Energy, 2009.
[2] D. G. Dorrell, M. Popescu, L. Evans, D. A. Staton, and A. M. Knight, "Comparison of permanent magnet drive motor with a cage induction motor design for a hybrid electric vehicle," in *Proc. IEEE Int. Power Electron. Conf.*, Sapporo, Japan, Jun. 2010, pp. 1807–1813.
[3] D. G. Dorrell, M.-F. Hsieh, M. Popescu, L. Evans, D. A. Staton, and V. Grout, "A review of the design issues and techniques for radial-flux brushless surface and internal rare-earth permanent magnet motors," *IEEE Trans. Ind. Electron.*, 2011, DOI: 10.1109/TIE.2010.2089940.
[4] D. G. Dorrell, M. Popescu, L. Evans, D. A. Staton, and A. M. Knight, "Comparison of different motor design drives for hybrid electric vehicles," in *Proc. IEEE Energy Conv. Congr. Expo.*, Atlanta, GA, Sep. 2010, pp. 3352–3359.
[5] D. G. Dorrell, M. Popescu, L. Evans, D. A. Staton, and A. M. Knight, "Modern electrical machine analysis and design techniques applied to hybrid vehicle drive machines," in *Proc. IEEE Int. Symp. Ind. Electron.*, Bari, Italy, Jul. 4–7, 2010, pp. 3728–3733.
[6] K. I. Laskaris and A. G. Kladas, "Internal permanent magnet motor design for electric vehicle drive," *IEEE Trans. Ind. Electron.*, vol. 57, no. 1, pp. 138–145, Jan. 2010.
[7] W. Hua, M. Cheng, and G. Zhang, "A novel hybrid excitation flux-switching motor for hybrid vehicles," *IEEE Trans. Magn.*, vol. 45, no. 10, pp. 4728–4731, Oct. 2009.
[8] M. Eberhard, "How electric vehicles must change the way the auto industry thinks," in *Proc. IEEE ECCE Conf. Plenary Session*, San Jose, CA, Sep. 24–28, 2009.
[9] Y. Takano, M. Takeno, T. Imakawa, A. Chiba, N. Hoshi, M. Takemoto, and S. Ogasawara, "Torque density and efficiency improvements of a switched reluctance motor without rare earth material for hybrid vehicles," in *Proc. IEEE Energy Conv. Congr. Expo.*, Atlanta, GA, Sep. 2010, pp. 2653–2659.
[10] Y. Takano, M. Takeno, N. Hoshi, A. Chiba, M. Takemoto, S. Ogasawara, and M. A. Rahman, "Design and analysis of a switched reluctance motor for next generation hybrid vehicle without PM materials," in *Proc. Int. Power Electron. Conf.*, Sapporo, Japan, Jun. 21–24, 2010, pp. 1801–1806.
[11] R. McCormack, "China's complete control of global high-tech magnet industry raises U.S. national security alarms," *Manufacturing and Technology News*, vol. 16, no. 16, Sept. 30, 2009 [Online]. Available: http://www.manufacturingnews.com/news/09/0930/magnets.html
[12] J. A. Walker, D. G. Dorrell, and C. Cossar, "Flux-linkage calculation in permanent-magnet motors using the frozen permeabilities method," *IEEE Trans. Magn.*, vol. 41, no. 10, pp. 3946–3948, Oct. 2005.
[13] J. R. Hendershot and T. J. E. Miller, *Design of Brushless Permanent-Magnet Motors*. Oxford, U.K.: Clarendon Press, 1994.
[14] T. J. E. Miller, "SPEED's Electrical Motors," SPEED Laboratory, University of Glasgow, Glasgow, U.K., 2006.